Studia Geophysica et Geodaetica (2026) 70:7
https://doi.org/10.1007/s11200-026-00016-7

Magnetic Signature of the Camarena de la Sierra Jurassic Magmatism in the SE Iberian Chain (Teruel, Spain)

Belén Oliva-Urcia[1] · **Antonio Cassas-Sainz**[1]

Received: 30 June 2025 / Accepted: 16 September 2025

Abstract

Magnetic fabrics are commonly studied to understand the magma flow in volcanic and hypovolcanic settings. In this work we present a magnetic fabric study in the Sierra de Javalambre (SE Iberian Chain), a geological unit that includes a swarm of Mesozoic volcanic intrusive and extrusive bodies associated with a hotspot and extensional deformation in Eastern Iberia during the Mesozoic. The sill sampled in this work is constituted by alkaline dolerites (ocean island basalts, OIB composition) and is a part of more than a hundred outcrops emplaced in Upper Triassic (Keuper facies) diapiric units and Jurassic limestones. The presence of Ti-poor titanomagnetite in the studied hypovolcanic rocks is inferred from temperature-dependent magnetic susceptibility curves and also from analyses of the three components isothermal remanent magnetization (IRM), since the decay of the magnetic susceptibility and the soft axis (0.12 mT) of the IRM occurs at 580°C. The magnetic susceptibility shows high values, in average 17554×10^{-6}. The anisotropy of the magnetic susceptibility shows some dispersion of the maximum and intermediate axes on the bedding plane, whereas the minimum axes are clustered almost perpendicular to the bedding plane for the 158 standard analyzed samples. The magnetic lineation (clustering of the maximum axes of the anisotropy of magnetic susceptibility) is bimodal with WNW-ESE and NNE-SSW directions in the in-phase magnetic susceptibility, and can be interpreted as the flow direction of the magma controlled by the NW–SE and N-S extensional fault systems during the basinal (Jurassic) stage.

Keywords Magnetite · Sill · Igneous · Hypovolcanic

✉ Belén Oliva-Urcia
boliva@unizar.es

Antonio Cassas-Sainz
acasas@unizar.es

[1] Geotransfer-IUCA, Ciencias de La Tierra, Universidad de Zaragoza, C/Pedro Cerbuna 12, 50009 Saragossa, Spain

Published online: 02 April 2026

1 Introduction

Magnetic fabric in igneous rocks has been used to infer the magma flow, particularly in cases where the magma source is eroded, in order to infer the position of such magma foci. This is the case for example of the study of the volcaniclastic deposits ejected by ancient volcanoes that at present are not easy to locate, as in the Late Carboniferous-Permian volcaniclastic series in the Pyrenees (Simón-Muzás et al., 2022) or in other cases where the magmatic source does not crop out, such as dykes or sills. Many studies have been carried out in dykes and lava flows to understand on one hand the position of the magma source, and on the other hand the development of "anomalous" magnetic fabrics, which are magnetic fabrics where the magnetic axes of the magnetic ellipsoid do not follow the main structural planes, such as the dyke planes or depositional surfaces in lavas (when present) (Cañón-Tapia, 2004; Cañón-Tapia et al., 1997; Cañón-Tapia and Pinkerton, 2000; Das and Malik, 2020; Gil-Imaz et al., 2012; Raposo, 1997; Simón-Muzás et al., 2023; Soriano et al., 2016 among many others). In addition, the anisotropy of magnetic susceptibility (AMS) has been also used to disentangle flow-induced shear in lavas when the magma source and lavas are preserved (Caballero-Miranda et al., 2016). Sills have been also studied using AMS as a tool to decipher the flow dynamics and magma migration in the upper crust. In these studies the influence of thermal contraction has been observed to affect the magnetic fabric (Gil-Imaz et al., 2006; Hrouda et al., 2015). Therefore, authors recommend caution in the solely use of AMS to infer magma flow, because regional trends may differ from the ones obtained in different portions of the sill depending on the sill geometry (Hoyer and Hasstie, 2022). In some sills magnetic fabrics are described as highly variable over small distances, and it is interpreted as due to horizontal flow restriction within growing sills (Martin et al., 2019). In other investigations AMS is also compared to other proxies of flow, such as the shape preferred orientation (SPO) of plagioclase crystals, or intrusive steps and magma lobes (Ferré et al., 2002; Hoyer and Watkeys, 2017). However, more homogeneous orientation of magnetic lineations (ca NW or SE) indicating magma flows in dolerite sills and dykes have also been obtained (Elming and Mattsson, 2001 and references therein).

Our interest in a small section of the Mesozoic dolerite sills in the Javalambre Sierra of the SE Iberian Chain (NE Spain) is to decipher the orientation-distribution of minerals obtained by the AMS or magnetic fabric, and their relationship to the Mesozoic rifting episodes in the Iberian Basin. The magnetic fabric analyses go hand in hand with standard rock magnetic analyses to decipher the main carrier(s) of the magnetic fabric. Optical microscopy observations and X-Ray diffraction analyses were also conducted in few samples to better constrain the mineralogical phases and their distribution.

2 Geological Setting

The studied alkaline dolerites form part of a significant igneous system whose importance in terms of the geodynamic evolution of the Iberian plate and the western Tethys has been underlined in previous works (Cortés, 2020, 2023;

Lago-San José et al., 2000; Ortí-Cabo and Vaquer-Navarro, 1980). These well-known outcrops are located in the SE Iberian Chain, in the Javalambre Sierra, near the Camarena de la Sierra village (~2 km SE of the village).

The volcanic and subvolcanic rocks that form this igneous system are interbedded within the Triassic and Jurassic units of the Iberian Chain, an intraplate range resulting from the Alpine (mainly Paleogene) inversion of the Mesozoic intracratonic Iberian Basin. The geometry and structural trend of the intracratonic rift system are partly inherited from Variscan structures (Aurell et al., 2019; De Vicente and Vegas, 2009; Liesa et al., 2018). The Mesozoic rifting is divided in two main phases: the first stage is related to the deposition of Permian and Triassic units and the second major phase of tectonic subsidence occurred during the Late Jurassic—Early Cretaceous (García-Lasanta et al., 2015; Martín-Martín et al., 2013 and references therein). This second rifting phase in the Iberian Basin coincides with the rift propagation from the Middle Atlantic towards the north and the opening of the Bay of Biscay (Ziegler, 1990). During the same period, the opening of the Tethys Ocean resulted in an heterogeneously distributed stretching which in turn generated a constantly thinned domain in the Iberian Intraplate realm, where "coeval rift-related deformation and rift-drift transitions migrated significantly along space and time" (Aurell et al., 2019; García-Lasanta et al., 2016 and references therein).

The volcanic, subvolcanic and volcaniclastic materials of the SE Iberian Chain interbedded within the Pliensbachian to Toarcian sediments, which were deposited in shallow marine platforms (Cortés, 2020; Valenzuela-Ríos et al., 1996). The ages of intrusions have been constrained between the Pliensbachian (Early Jurassic) and the Bajocian (Middle Jurassic), within a period of circa 20 Ma (Cortés, 2023). Igneous outcrops occur along the Caudiel and Alcublas fault zones, that are linked to NW–SE faults (Gómez and Fernández-López, 2006; Ortí-Cabo and Vaquer-Navarro, 1980). In fact, these faults have been interpreted from the alignment of volcanic, subvolcanic and volcaniclastic materials and differences in thickness of the sedimentary sequences. A maximum subsidence has been proposed during the Early Jurassic, at least in the Alcublas fault zone (Ortí-Cabo and Vaquer-Navarro, 1980).

The post-rift evolution of this sector of the basin is pinpointed by the formation of folds and thrusts with different orientations during the Cenozoic tectonic inversion, from N-S to NE-SW and NW–SE (De Vicente et al., 2009; García-Lasanta et al., 2016; Liesa et al., 2018; Nebot Miralles and Guimerà, 2016).

Some of the NW–SE Jurassic and probably Triassic faults (Ortí-Cabo and Vaquer-Navarro, 1980) played a relevant role during the Mesozoic evolution of the area, particularly, the ATMU (Alto Tajo-Montes Universales) fault system with NW–SE orientation, parallel to the Caudiel and Alcublas fault zones (Fig. 1). The sedimentological record indicates that the activity of the ATMU fault during the Jurassic separates the area where shallow marine carbonates (west of the ATMU system) occur from the open marine sediments (east of the ATMU fault system) accumulated. The Landete-Teruel (LT) Fault, belonging to the fault system almost perpendicular to the former one (NE-SW orientation) was active from the mid-Kimmeridgian onwards and also affects the sedimentological environment during the Mesozoic, controlling the western extension of the marine sedimentation area (Aurell et al., 2019 and

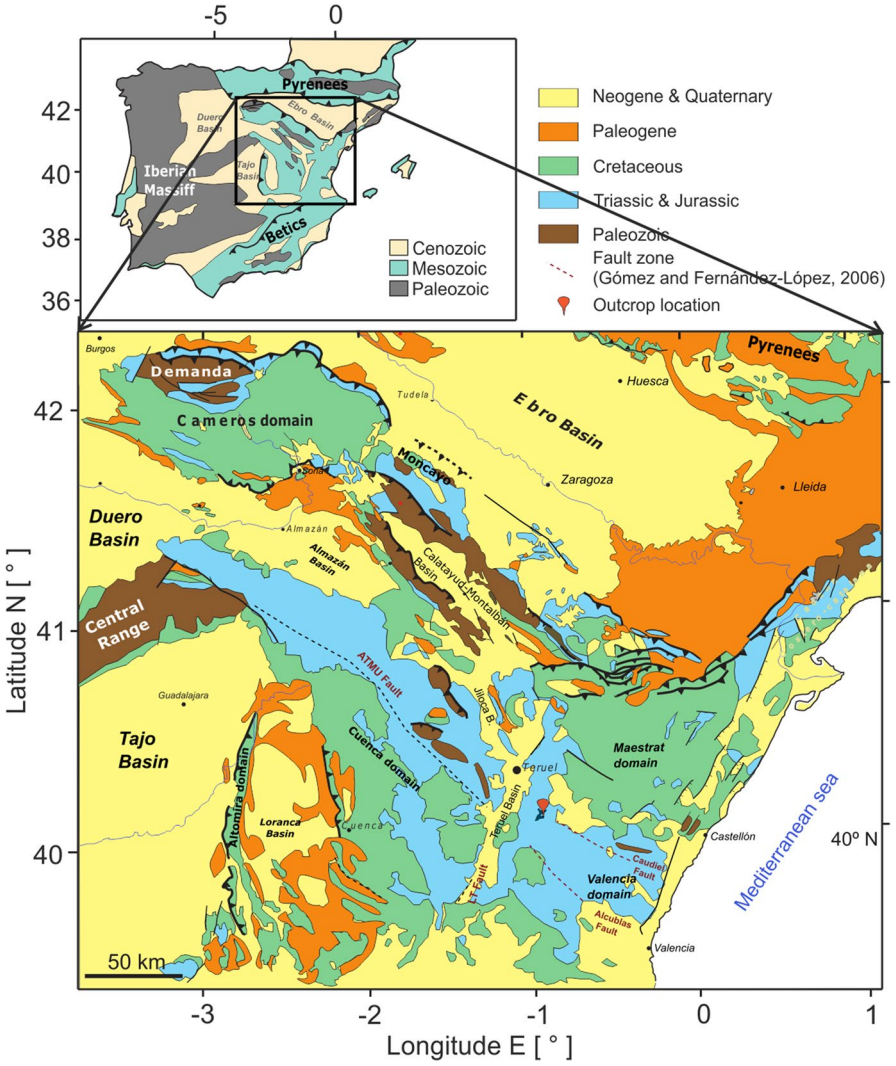

Fig. 1 Geological map with the location of the sampled outcrop in the SE Iberian Chain. Modified from Liesa et al. (2018); Aurell et al. (2019); Cortés (2023); De Vicente et al. (2009)

references therein), the rupture of the shallow platform and the compartmentalization of the basin since the Late Jurassic onwards.

In relation with the more recent tectonic evolution, the outcrop sampled in this work (Fig. 1) is located on the eastern margin of the Teruel basin, which is an asymmetric N-S graben formed during Miocene times (Anadón et al., 2004; De Vicente et al., 2009; Ezquerro et al., 2012) and also conditioned by inherited structures, that were re-activated during this stage. Regarding the geochemical information of the igneous rocks in the Valacloche-Camarena area, studied in this work, Lago San José

et al. (2000) determined that the samples are relatively evolved alkali basalts with a compositional pattern similar to a typical OIB (ocean island basalt). In the Camarena de la Sierra area, dolerites show a more evolved geochemical composition respect to the Valacloche area (~4 km to the NW of Camarena area). Some fluidality structures are seen at the top of the sills, which also have crustal enclaves (prevailing those with compositions from the upper crust). The absence of high temperature metamorphism indicates, together with the fluidality structures, subvolcanic conditions for the emplacement of the sills. This magmatism (considered as Triassic, pre-Hettangian, by these authors and Jurassic by the above-mentioned ones) is exposed in more than a hundred outcrops within seven areas (some of them linked to salt tectonics (Ortí-Cabo and Vaquer-Navarro, 1980) in the Iberian Chain (see Fig. 1b in Lago San José et al., 2000).

3 Methods

The sampled outcrop is a sill dolerite, along ~50-m section along the road TE-34, 2 km to the SE of Camarena de la Sierra village (Teruel, Spain). A total of 35 cores were drilled with a gasoline powered drill machine (distributed in three sites), refrigerated with water. Besides, five oriented hand samples were taken (one in IS-1, two in IS-2 and two in IS-3). Cores were oriented with a clinometer. A total of 101 standard cylinder samples of about 10 cm^3 were cut with a double saw machine in the laboratory and 57 cubic samples of about 8 cm^3 were cut from the five oriented hand samples (10 cubic samples in IS-1 around IS-1 10 core, 12 cubic samples from IS-2A, 14 cubic samples from IS-2B, 12 cubic samples from IS-3A and nine cubic samples from IS-3B). The AMS was measured in a KLY5 Kappabridge using the 3D rotator (1 position) and the standard rotator (3 positions) under a peak field of 400 A m^{-1} and an operating frequency of 1220 Hz, at room temperature at the University of Zaragoza. The KLY5 susceptometer (AGICO Inc.), also allows to extract the out-of-phase magnetic susceptibility, in addition to the standard in-phase magnetic susceptibility information. The phase angle (δ), is obtained as $tan\delta = k\prime/k''$, where $k\prime$ and k'' are the ipMS (in-phase magnetic susceptibility) and opMS (out-of-phase magnetic susceptibility) components, respectively. It is recommended for the phase angle to be higher than 1° and also it is necessary to know the origin of the opAMS, i.e., to determine whether it is due to viscous relaxation, eddy currents, or weak field hysteresis (Hrouda et al., 2022). The Anisoft 5 software (Chadima et al., 2020) was used to visualize and compute the AMS parameters and orientation of the magnetic ellipsoid.

The anisotropy of magnetic susceptibility is a second rank tensor represented by an ellipsoid. Different parameters are used to describe the shape, degree of anisotropy and orientation of the axes of the ellipsoid. The more common parameters are the corrected anisotropy degree (Pj) and the shape parameter T, given as

$$Pj = P\prime = exp\left(\sqrt{2\left[\left(n_1 - n_m\right)^2 + \left(n_2 - n_m\right)^2 + \left(n_3 - n_m\right)^2\right]}\right), T = \frac{2n_2 - n_1 - n_3}{n_1 - n_3},$$

where $n_1 = ln\kappa_{max}$, $n_2 = ln\kappa_{int}$, $n_3 = ln\kappa_{min}$, and $n_m = \left(n_1 + n_2 + n_3\right)/3$. The shape parameter varies from 0 to 1 in oblate ellipsoids and from –1 to 0 in prolate ellipsoids (Jelínek, 1981). The orientation of the three axes of the ellipsoid is analyzed considering the main structural surfaces, in this case the bedding plane.

Six samples were cooled down immersed in liquid nitrogen (~77 K) and measured manually in 15 positions in the KLY3 susceptometer (AGICO Inc.) following the procedure of Lüneburg et al. (1999). This procedure allows to estimate the carrier of the susceptibility. A perfect paramagnetic material will show an increase in the magnetic susceptibility at low temperature (77 K) by a factor of 3.8 with respect to the room-temperature value (Parés and van der Pluijm, 2002, 2014). Thermomagnetic curves of the temperature dependent magnetic susceptibility were analyzed in 10 samples from room temperature to 700°C. In two of these samples, a heating curve from –190°C to room temperature was also analyzed in the KLY3-CS and KLY3-CL instruments, in argon atmosphere. The Cureval 8 software (Hrouda, 2003; Chadima and Hrouda, 2009) was used to visualize and analyze the reversibility and the paramagnetic fraction present. Furthermore, Hrouda (2003) proposed a method for assessing the alteration of volcanic rocks. We use the A_{40} and A_{max} parameters, defined as:

$$A_{40} = \frac{k_{40} - K_{40}}{K_{40}}[\%], A_{max} = \frac{max(k - K)}{K_{40}}[\%], \quad (1)$$

where k_{40} is the magnetic susceptibility at 40 °C on the cooling curve, and K_{40} is the magnetic susceptibility at 40 °C on the heating curve. In the case of A_{max}, the maximum difference between values measured temperature on the cooling and heating curves is considered. Nine samples were thermally demagnetized as pilot samples. In other five samples, the "Lowrie test", or three-components test of isothermal remanent magnetization (IRM), applying three different magnetic fields, 1.9, 0.4 and 0.12 T along three different axes of a sample, and thermally demagnetizing the sample, was performed (Lowrie, 1990). These analyses were carried out at the Paleomagnetic Laboratory of the University of Burgos (Spain) with a TD-48 dual-chamber thermal demagnetizer (ASC Scientific), a JR-6 spinner magnetometer (AGICO Inc.) and a pulse magnetizer M2T-1 (Ferronato). From these parameters, the *Köenigsberger (1938)* ratio Q, was calculated according to its definition as the ratio of the natural remanent magnetization (M_R or NRM) to the induced magnetization (M_I) in the Earth's field

$$Q = \frac{M_R}{M_I} = \frac{NRM}{\kappa H_0}, \quad (2)$$

where κ is the bulk volume susceptibility and H_0 is the ambient magnetic field intensity.

Furthermore, paleomagnetic components were obtained during the demagnetization. In spite of the bad quality of the result, they have produced some constraints on the age of these rocks (or rather of the acquisition of magnetization) using the intersection of the demagnetization great circles. The results of the pilot thermal demagnetization procedure of nine samples are shown in the supplementary material.

Optical microscopy observations were done in 4 thin sections and ImageJ was used on the opaques minerals in one thin section to obtain the main orientation distribution. The ImageJ is a public domain Java image processing program (https://imagej.net/).

X-Ray diffraction analyses were also conducted in 7 samples in the Diffraction X-Ray Analyses by Fluorescence of the Research Support Service of the University of Zaragoza (SAI-unizar). A Ru2500 diffractometer from RIGAKU performed XRD measurements using a graphite monochromator to select the Cu Kα radiation between 3° and 80° 2Θ at a scan rate of 0.04° s^{-1} and 0.04° scan step. To determine the mineralogical phases the JCPDS- International Centre for Diffraction Data-2000 was used (results in supplementary material).

4 Results

The values of the magnetic susceptibility are high (the mean is $17{,}300 \times 10^{-6}$), accordingly to the volcanic mafic nature of rocks, but with an extremely wide range (between 100 and $80{,}100 \times 10^{-6}$). The results for each sample is presented in Table S1 of the Supplementary Material. The mean corrected anisotropy degree is 1.013 and the mean shape parameter T is 0.214 (oblate), both with strong variability. The natural remanent magnetization (*NRM*) of nine samples provide values between 0.04 and 0.35 A m^{-1} (see Table S2 and Fig. S1 in the Supplementary Material). The Köenisberger ratio Q, considering an intensity of 35.8 A m^{-1} for the Earth's magnetic field in Camarena de la Sierra for the nine demagnetized samples, is lower than 1. The average and standard deviation values of the AMS parameters can be seen in Table 1 and Fig. 2.

4.1 Rock Magnetism

Regarding the magnetic mineralogy, if we look at the temperature-dependent magnetic susceptibility curves, all samples have a positive alteration index A_{40} (Hrouda, 2003) since the cooling curves end at higher magnetic susceptibility than the heating runs start at (see Table 2 for the index of alteration A_{40}, Eq. (1) and Hrouda, 2003). That is, all curves are irreversible, indicating the occurrence of chemical changes during the experiment. The thermomagnetic curves of some of the samples suggest the presence of different ferromagnetic phases because in the heating run there

Table 1 Values of magnetic susceptibility (κ), anisotropy degree *Pj* and shape factor *T* (Jelínek, 1981). The values were determined from measurements of a total of 158 samples

	κ ($\times 10^{-6}$)	*Pj*	*T*
Mean	17300	1.013	0.252
Median	9965	1.010	0.316
Standard Deviation	20960	0.011	0.427
Minimum	100	1.002	–0.871
Maximum	88100	1.068	0.960

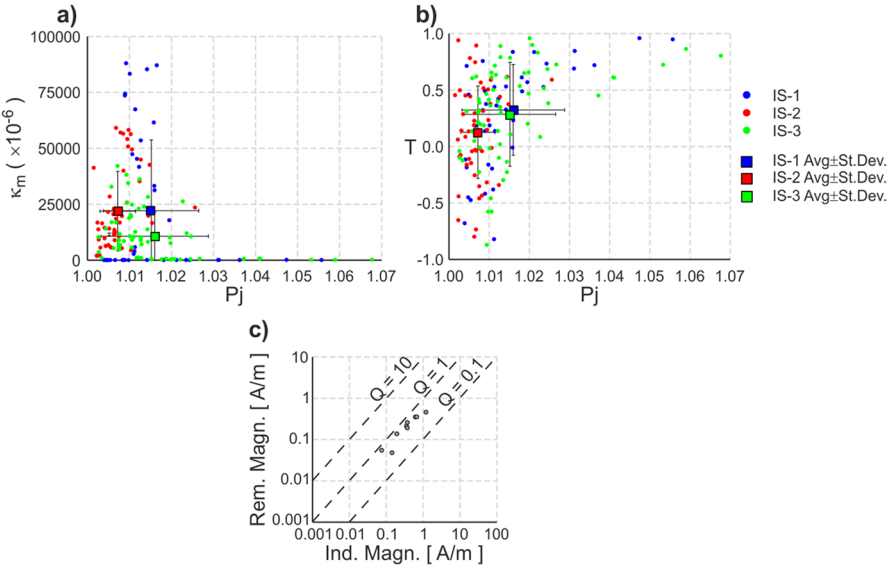

Fig. 2 Magnetic properties of the analyzed samples: **a)** volume-specific mean susceptibility κ_m in dependence of the anisotropy degree *Pj*, **b)** shape parameter *T* vs. *Pj* for all 158 samples; their average values with standard deviations are shown by big squares and bars, respectively; and **c)** remanent vs. induced magnetization with lines for different Köenigsberger ratio *Q* calculated for nine samples

is an increase of the magnetic susceptibility (hump) around 300 °C, a slight decay at higher temperatures and a final decay at 600 to 645 °C (Table 2, Fig. 3a). This behavior is found in IS-1–1, IS-2–2, IS-2–5 and IS-3–12. In IS-2–4 and IS-2–8 the hump at 300 °C is subtle, and the final decay occurs at 580 or 584 °C, what is typical of Ti-poor titanomagnetite. The 300 °C hump has been attributed to the inversion of maghemite to either hematite or titanomagnetite, or more recently to single domain magnetite undergoing stable single-domain (SSD) to super-paramagnetic (SP) transition (see references in Zhang and Appel, 2023). Samples IS-1–13 and IS-1–8 show a similar behavior with only a clear final decay at about 560 °C, typical of Ti-poor titanomagnetite. Conversely, the sample IS-3–10 also shows a strong decay at about 100 °C possibly due to Ti–rich titanomagnetite. The paramagnetic contribution was calculated in four samples (two of them in the lower temperature range, between –180 and –100°C). This contribution ranges from 66% to 81.3%. In the low-temperature curves, there is no clear Verwey transition (typical for multi-domain (MD) magnetite). On the contrary, a strong decay occurs in IS-2–4 LT until –180°C. This information is complemented with the three-components IRM test (Lowrie, 1990) (Fig. 3b). In all samples the low-coercivity component dominates the remanence; in four samples this component is titanomagnetite (with low Ti content), since the final decay of the remanence occurs below 580°C. In samples IS-2-4C and IS-2-3A some medium and high coercivity component is present, and there is a decay at about 350 °C). However, no hematite is found since there is no decay of the high-coercivity component at 680°C. Only sample IS-3-13B shows a decay at 300 °C, suggesting the presence of Ti–rich titanomagnetite, since the *k-T*

Table 2 Values from the curves of temperature dependence of magnetic susceptibility, used to determine the alteration parameters A_{40} and A_{max} (Eq. (1), Hrouda, 2003), and Curie temperature T_C, assessed using the inverse values in the paramagnetic temperature range (Petrovský and Kapička, 2006). The paramagnetic contribution was determined, where possible, by the Cureval 8 software from the inverse susceptibility of the heating curve

Sample	K_{40} ($\times 10^{-6}$)	k_{40}	T_{max} [°C]	$k-K$ at T_{max} ($\times 10^{-6}$)	A_{40}	A_{max}	T_C [°C]	T_C heat	T_C cool	Paramag [%]
IS-1–1	1600	1933	440	716	20.81	44.75	640	––	––	0
IS-1–13	2.86	9.9	40	––	246.15	––	564	40	300	81
IS-1–8	5.64	16.9	40	––	199.65	––	555	40	300	68
IS-1-A	2.8	17.06	200	16.4	509.29	585.71	575	100	300	80
IS-2–2	492	774	40	––	57.32	––	644	––	––	0
IS-2–4	5.6	176	346	232	214.29	414.29	580	–160	–100	67*
IS-2–5	252	416	380	232	65.08	92.06	600	––	––	0
IS-2–8	100	238	350	226	138.00	226.00	587	––	––	0
IS-3–10	15	20	240	18	33.33	120.00	564	120	40	–99?
IS-3–12	405	629	430	298	55.31	73.58	645	––	––	0
IS-3–17	6.4	16	210	15	150.00	234.38	600	–180	–120	70*

* Determined using low-temperature curves

experiments of a nearby sample IS-3–12 does not show iron sulphides in the κ-T analyses. Indeed, iron sulphides have a Curie temperature of 330 °C (Dunlop and Özdemir, 1997; Kontny et al., 2000) that cannot be interpreted from our curves.

The suggested relative high content of magnetite in many samples is consistent with the measurements of magnetic fabrics at liquid nitrogen temperature (~77 K), that indicate a significant contribution of the ferromagnetic phase to the total susceptibility. Indeed, the magnetic susceptibility only increases 1.5 times with respect to the value measured at room temperature (Fig. 3c). In summary, the main carriers of the AMS seem to be Ti-poor titanomagnetite, paramagnetic minerals and some Ti–rich titanomagnetite.

4.2 Magnetic Fabrics

The orientation of the magnetic ellipsoid (AMS) shows a cluster of the maximum axes of the ellipsoid along a NNE-SSW direction in geographic coordinates, located within or close to the bedding plane, in IS-1. Conversely, IS-2 shows quite disperse axes but κ_{max} closer to the vertical. Finally, IS-3 shows the κ_{max} axes in a girdle distribution with κ_{int} axes, the girdle defining a nearly vertical plane (Fig. 4 and Table 3). A secondary maximum of the magnetic lineation appears in E-W direction, also horizontal, when the beds are restored to the horizontal. In general, the axes of the magnetic ellipsoid are not well grouped, and confidence angles for κ_{max} are higher than ~ 57°, whereas for the κ_{min} there is a range from ~ 16° to 48°. The out-of-phase diagrams show directions for the magnetic axes similar to the ones observed

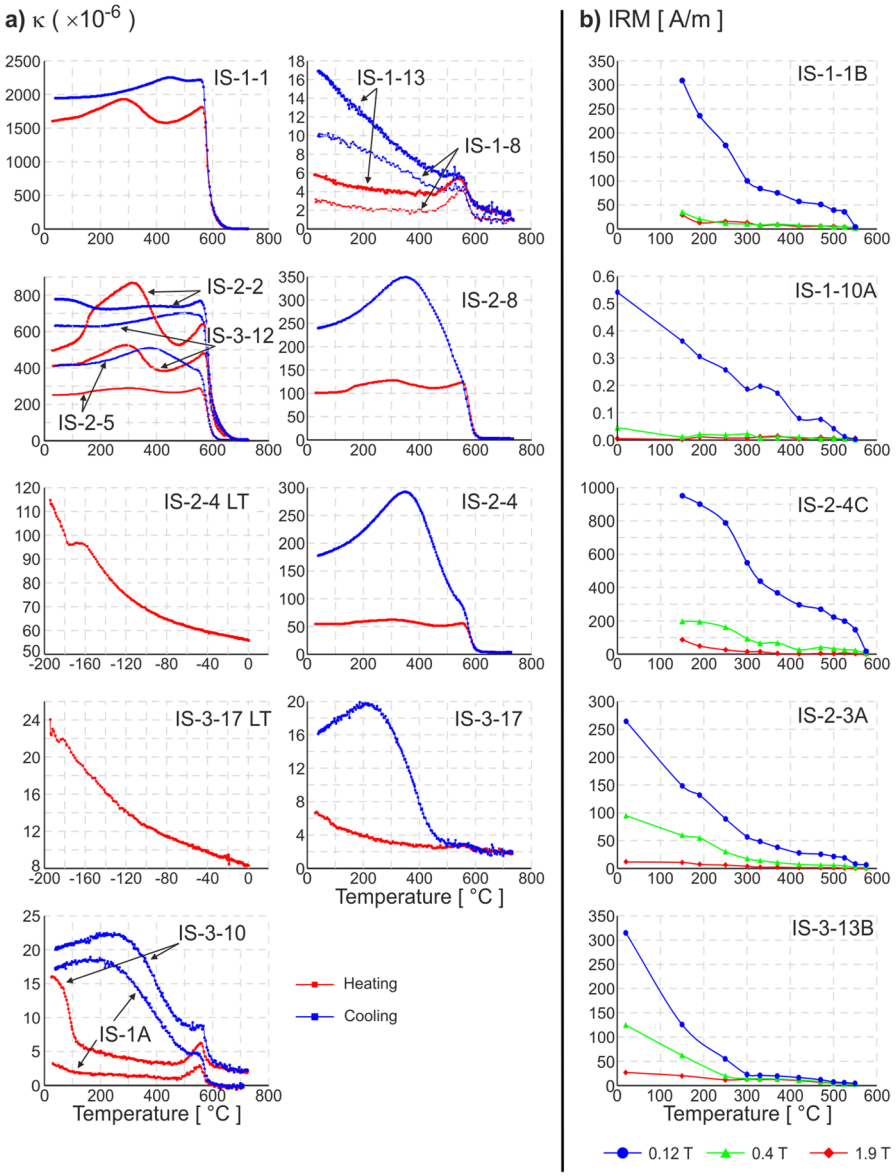

Fig. 3 **a)** Temperature dependence of magnetic susceptibility κ, and **b)** three-component test of isothermal remanent magnetization (*IRM*) according to Lowrie (1990). In case of two samples (IS-1-1B and IS-2-4C), the steps at low temperatures, when magnetization was out of scale of JR-6 magnetometer, are not shown. See next page for Fig. 3c. **c)** Low-temperature (LT) vs. room-temperature (RT) magnetic susceptibility for samples in Table S3 of Supplementary Material

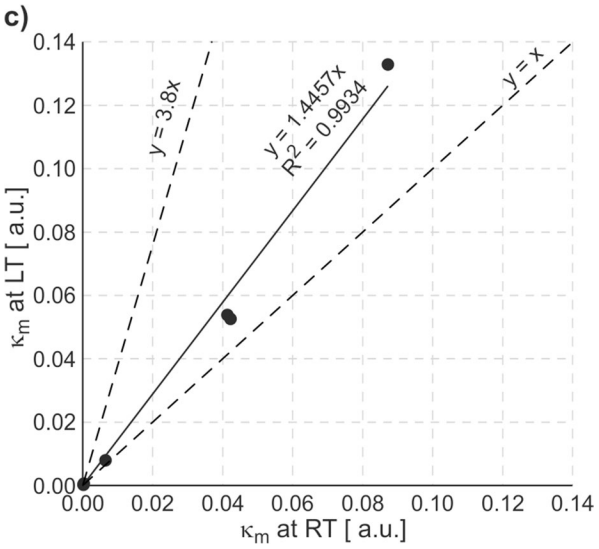

Fig. 3 (continued)

for the in-phase diagrams. Particularly, axes are better grouped for the out- of-phase stereoplot in sites IS-2 and IS-3.

The plots of κ_m, *Pj*-κ_m and *T*-*Pj* indicate the extreme variability of the bulk magnetic susceptibility in these samples, and the independence of *Pj* of magnetic susceptibility (Fig. 4). As mentioned before, oblate ellipsoids dominate, and the degree of the corrected anisotropy is stronger for more oblate ellipsoids, a trend that appears more clearly in IS-1 and IS-3 than in IS-2.

The position of sites within the subvolcanic body strongly conditions the results in terms of axes orientations. The lower part of the tabular sill shows the κ_{min} axes (IS-1) perpendicular to bedding (normal fabric), whereas in the middle part of the sampled section (IS-2), the maximum axes are close to the pole to bedding (and the out-of-phase stereoplot shows an inverse fabric in terms of axes disposition). In the upper part of the subvolcanic body (IS-3), the in-phase magnetic susceptibility shows the maximum axes of some samples (the ones with large $\kappa_m > 10^{-3}$),perpendicular to bedding, and the out-of-phase magnetic susceptibility shows orientations that approach an inverse fabric.

4.3 Optical Microscopy Observations and X-Ray Diffraction

The observation of 4 unoriented thin sections reveals the sericitized dolerites (Fig. 5). We observed a fine grained matrix of: quartz, altered Na-feldspars (plagioclase -albite-) and alkali (K)—feldspars (microcline and orthoclase), phyllosilicates

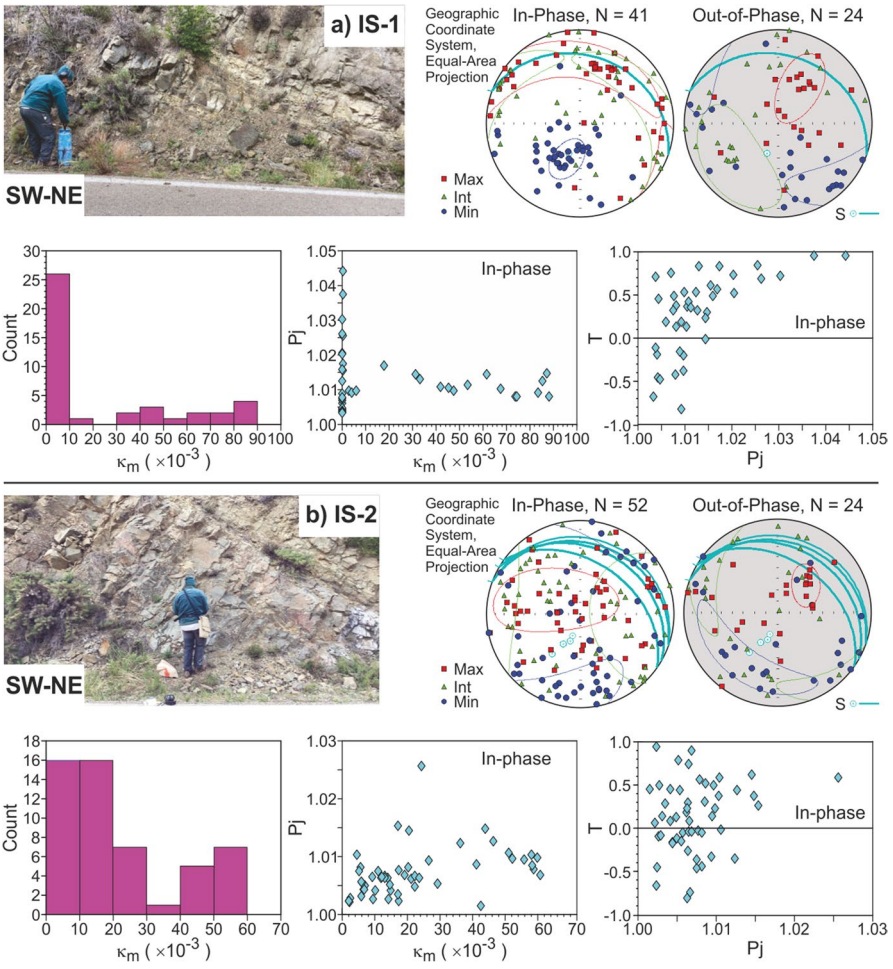

Fig. 4 Field pictures and the anisotropy of magnetic susceptibility results of samples listed in Table 3, obtained using Anisoft 5. Stereoplots for the out-of-phase data show data with the phase angle larger than 1. The thick blue great circles represent the orientation of the tabular disposition of the sill (S in the figure); κ_m – mean magnetic susceptibility, Pj – anisotropy degree, T – shape factor. See next page for third sample

(clinochlore), clinopyroxenes (diopside), olivine (in one sample a garnet is also present) and opaque minerals (Fe-Ti oxides) (Fig. 5b, c). In two samples some colored bands are observed (Fig. 5f, g). The results of the indentification of some mineral phases are in Fig. S2 of the Supplementary Material.

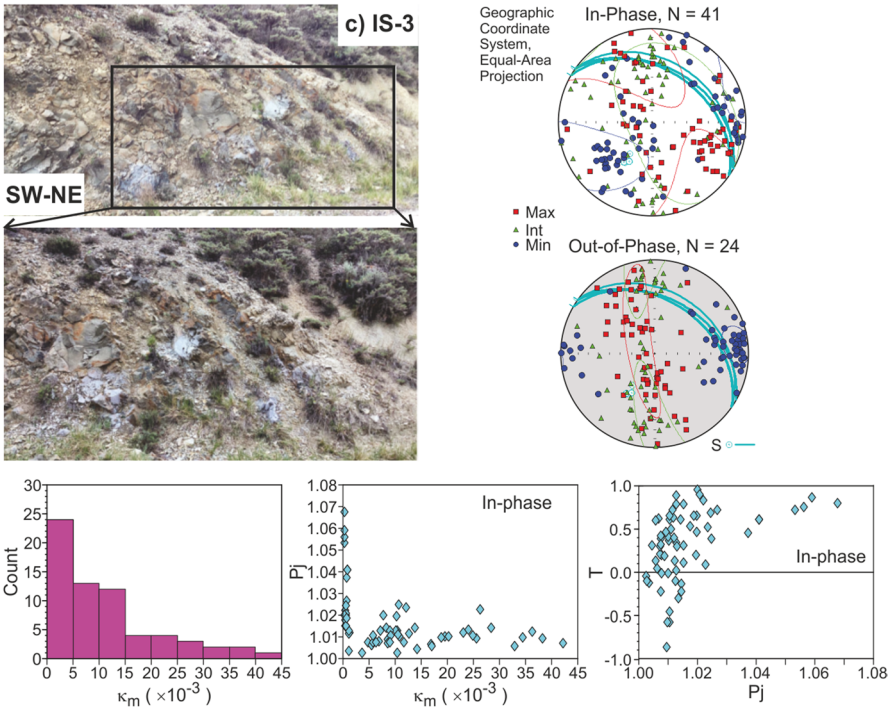

Fig. 4 (continued)

Table 3 Orientation of AMS ellipsoid for each site, in geographic coordinates, for in-phase (IP) and out-of-phase (OP) measurements of samples shown in Fig. 4 (only samples with the phase larger than 1 are considered); *N*—number of samples, *D*—declination, *I* – inclination, *α*—confidence angle

	Site	*N*	κ_{max}				κ_{int}				κ_{min}			
			D [°]	*α* [°]	*I* [°]	*α* [°]	*D* [°]	*α* [°]	*I* [°]	*α* [°]	*D* [°]	*α* [°]	*I* [°]	*α* [°]
IP	IS-1	41	350.0	87.2	29.9	17.7	87.7	87.2	13.9	16.4	199.6	20.7	56.0	12.3
	IS-2	52	298.4	57.7	62.7	27.1	92.6	57.7	24.9	48.3	187.5	49.2	10.4	23.9
	IS-3	65	332.9	77.8	11.1	28.4	85.0	77.8	62.5	47.8	237.7	49.4	24.8	25.2
OP	IS-1	24	30.9	34.9	52.7	27.1	92.6	57.7	24.9	48.3	132.7	45.9	18.9	18.9
	IS-2	24	46.1	18.8	55.2	12.4	307.5	60.0	5.9	14.4	213.5	60.1	34.1	16.0
	IS-3	57	311.1	71.2	71.2	11.0	176.9	71.8	13.3	12.6	83.8	126.0	13.0	12.4

The abundant opaque minerals (Fe-Ti oxides) show acicular (most abundant), prismatic and squared shapes (less abundant). The analyses of the orientation of the elongated opaque minerals in IS-2-B2 with ImageJ software (Fig. 5l) suggest a predominance of oriented minerals at 90° and ~ 50–150° with respect to the relative "north = upper part" of the unoriented thin section.

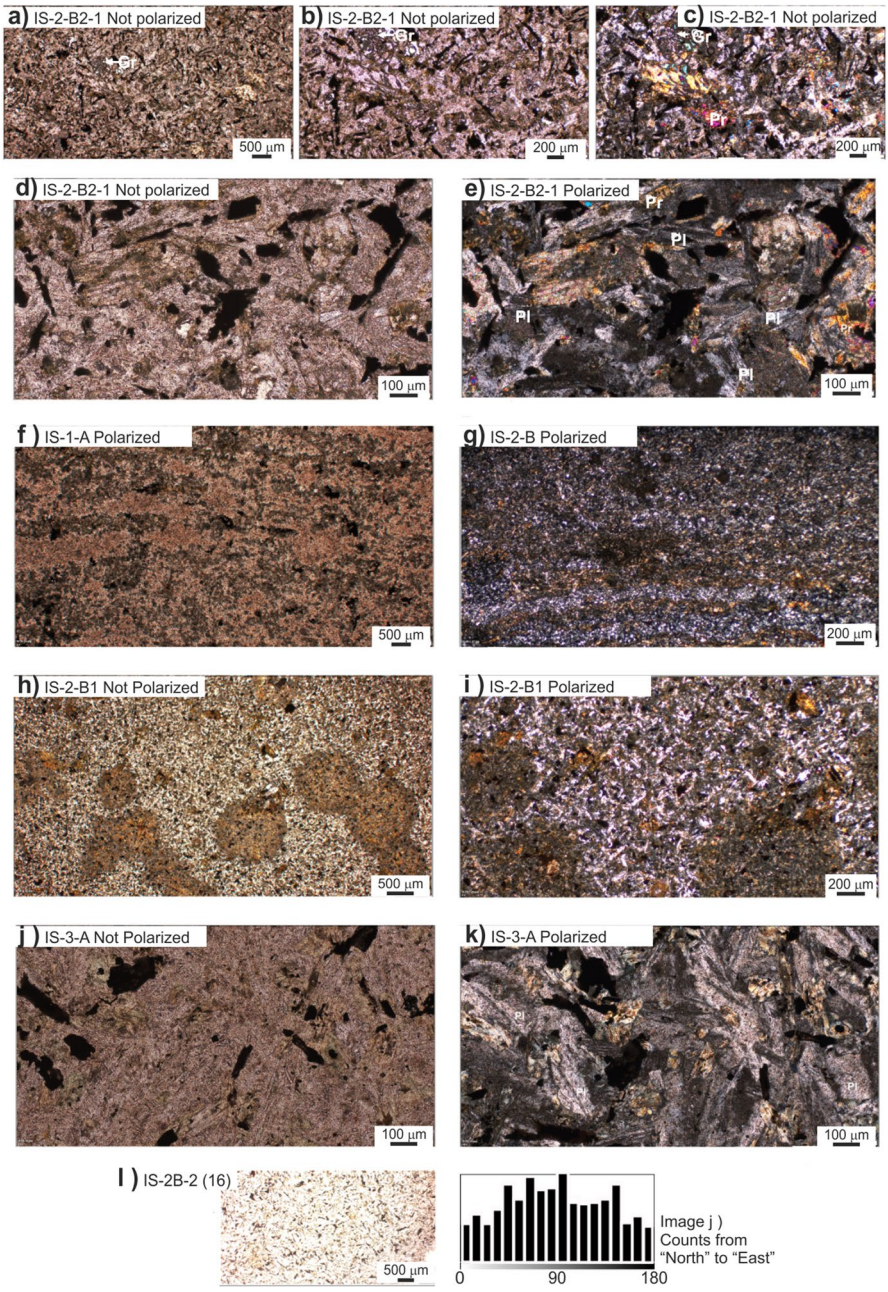

Fig. 5 Sericitized dolerites in thin section. Gr: garnet, Pl: plagioclase, Pr: pyroxene and opaques minerals (Fe-Ti oxides). North and East are only relative to the position of the thin section (North = upper part)

5 Discussion

The orientation of the magnetic ellipsoids can be used to interpret the flow dynamics and magma migration in the upper crust, both at surface and in hypovolcanic bodies (Simón- Muzás et al., 2022, 2023 and references therein). Indeed, magnetic fabrics in other igneous bodies in the Iberian Chain have been studied and interpreted as resulting from magmatic flow (Gil-Imaz et al., 2006; Majarena et al., 2017) in Late-Carboniferous and Permian rocks with little or no influence from deformational features during the subsequent Paleogene compression (Majarena et al., 2017). As a first approximation, the "normal" fabric is the one that shows the magnetic foliation plane (plane perpendicular to the κ_{min} axes) parallel to the bedding plane (or in some cases other structural surfaces) measured in the field (Chadima et al., 2006, see Fig. 6 for classification of magnetic fabric types). Therefore, data can be filtered according to the relationship between κ_{min} axes and the bedding plane. After eliminating sites with inclination of the κ_{min} axes lower than 60° (after tectonic correction), the averaged maximum axes show two maxima, the main one closer to an E-W direction (31 samples from the three sites), and the secondary one closer to a N-S direction (14 samples from the three sites). The rest of the samples (14) show more disperse orientations (Fig. 6).

The out-of-phase magnetic signal in IS-3 provides κ_{max} axes scattered with κ_{int} axes within a girdle perpendicular to κ_{min} axes that are oriented E-W (in geographic coordinates). It is close to an "inverse" type of fabric, with respect to the normal in-phase magnetic signal (considering the bedding plane as a reference). Therefore, the magnetic fabric is perhaps carried by stable single domain (SSD) particles (Hrouda et al., 2020).

Both the E-W and NNE-SSW magnetic lineation maxima are found in the three sites of the studied outcrop. Their orientation is oblique to the main structural features of the area that have a paleogeographical meaning: the NW–SE "Iberian" faults and the NE-SW "tethysian" faults (Fig. 6c) (García-Lasanta et al., 2016 and references therein). Furthermore, other fault trends can be considered within the extensional tectonic setting of the eastern Iberian Chain in Jurassic times, compatible with the main faults that control the extension and subsidence, namely the N-S set (that was subsequently re-activated during the Miocene extension in the Teruel graben). The N-S faults could be responsible for the conditioning of the magmatic flow in the soft levels (made up of Upper Triassic materials) below the surface during the Jurassic. Interestingly, AMS data from sedimentary layers within the Jurassic (Pueyo Anchuela et al., 2013) indicate paleocurrents in coastal sediments following the NNE- SSW direction (as indicated by one of the maxima found in their work), what is possibly related with the activity of faults in this direction (and consistent with a slightly deviated "Tethyan" extension).

The main orientations of the magnetic lineation found in a small percentage of the samples in Camarena de la Sierra outcrop show a quasi-perpendicular relationship in the three sites. This situation is quite different from the outcrops studied in Hoyer and Watkeys (2017), where they also find perpendicular relationships among AMS sites in a more detailed work in different outcrops near the sill contacts of the

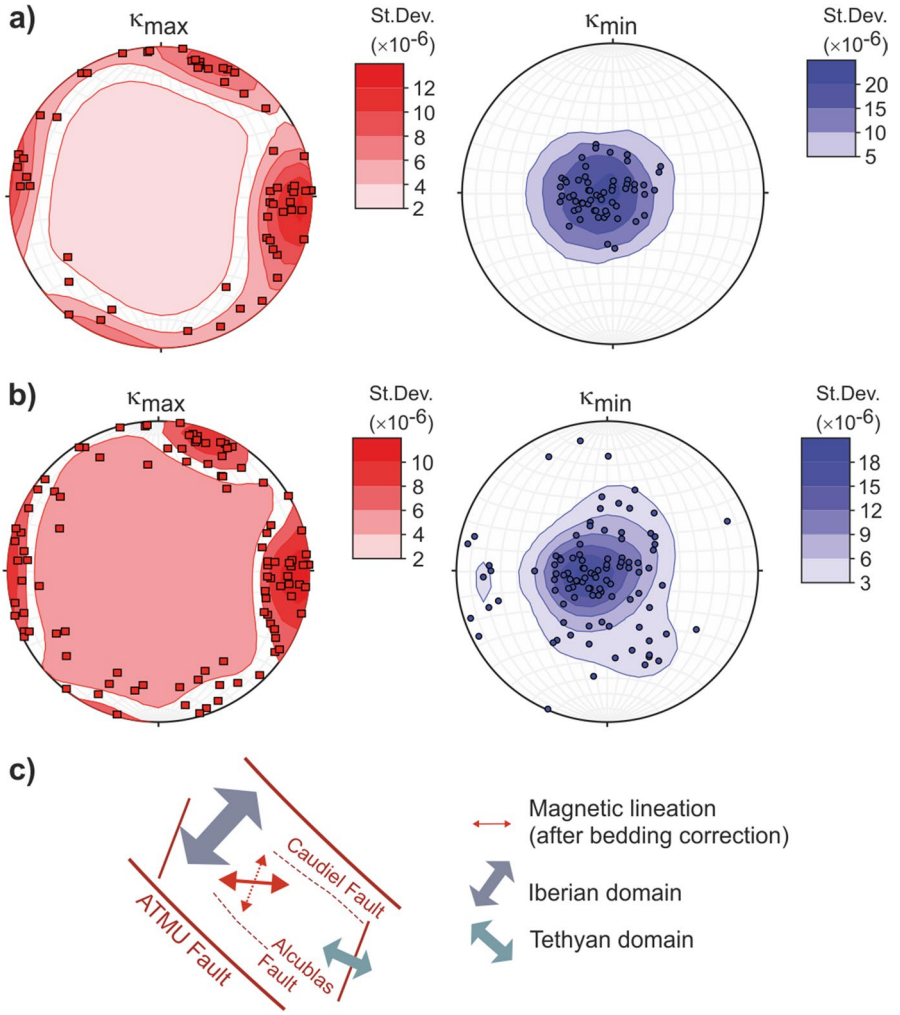

Fig. 6 Stereoplots of maximum and minimum susceptibility (κ_{max} and κ_{min}) axes after bedding restoration to the horizontal: **a)** 59 samples where κ_{min} axes have inclinations higher than 60° (Anisoft 5); **b)** 102 samples where κ_{max} axes have inclinations lower than 30° (Anisoft 5); **c)** simplified structural configuration for the Jurassic, compatible with the E-W orientation of magma flow (obtained from the magnetic fabric) in an area where Iberian and Tethyan extensional domains are present (thick arrows). The maxima of the magnetic lineation obtained in this study are represented (thin red arrows) and the main faults (ATMU, Caudiel, Alcublas faults) are shown

Karoo Igneous Province. Their interpretation, based also in macroscopic flow direction observed in the field, implies that the fabric follows the main flow direction of the magma when the sills segments are independent, but when the sills segments merge in a perpendicular direction to the magma flow, the sill segments coalesce and other orientation is imprinted in the AMS (mostly perpendicular but also chaotic).

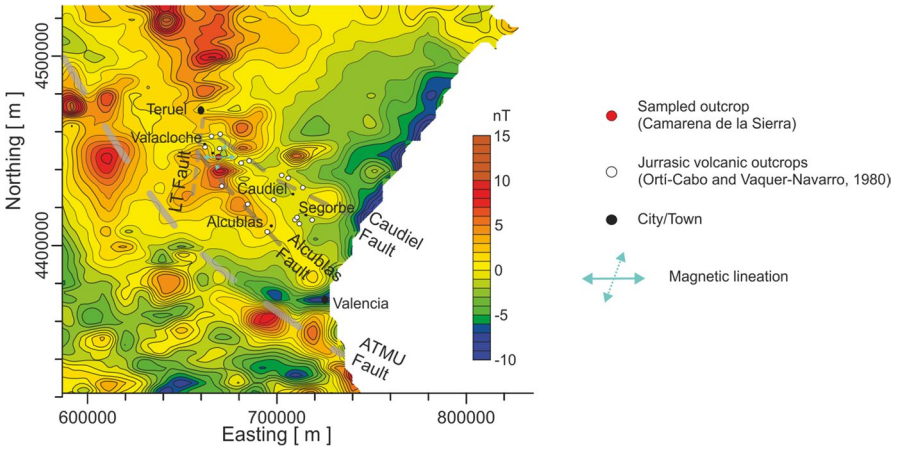

Fig. 7 Magnetic anomalies in the studied area. Base map: magnetic anomalies of the Iberian Peninsula. IGN, CC-BY 4.0 ign.es 2021 data provided by the Spanish National Geographic Institute (IGN). The maxima of the magnetic lineation obtained in this study are represented together with the main faults. Based on *Martí-Cabo* et al. *(1980)* and Aurell et al. (2019)

The values of magnetic susceptibility and remanence obtained in this work can explain some of the (subtle) magnetic anomalies found in the eastern Iberian Chain (Fig. 7). In our case, the subtle positive anomaly and the geometry of the dipole (Fig. 7) agrees with the lower Köenigsberger ratio of the samples, indicating that magnetic susceptibility (according to the strong values obtained in this work) controls the magnetic signal. The alignment of dipoles along a NW–SE direction following the Alcublas fault zone suggest the existence of a series of foci along this fault. The characterization in more detail of these anomalies from near-surface surveys could be of interest for determining the source of volcanic rocks as shown in other areas of the Iberian Chain (Calvín et al., 2014).

6 Conclusions

The magnetic analyses of a tabular dolerite sill in the Javalambre Sierra reveal the presence of Ti-poor titanomagnetite as the main carrier of the magnetic fabrics. Paramagnetic (pyroxene, phyllosilicates) and diamagnetic minerals represent a minor contribution to the total susceptibility. Ti–rich titanomagnetite and iron sulphides may be present in few samples, at the top of the sampled outcrop. The "inverse" out-of-phase fabrics of the upper part of the body could be carried by single domain particles as the out-of-phase signal suggests.

The "normal" in-phase magnetic anisotropy reveals an E-W and a NNE-SSW magnetic lineation, which may indicate the flow direction in the subvolcanic body. Thirty-one samples from the total of 158 (~20%) show the E-W lineation, whereas only 14 samples (~9%) present the NNE-SSW orientation. These directions are

compatible with the paleogeographic scenario during the Jurassic, conditioned in its turn by the main faults linked to extensional tectonics.

The magnetic susceptibility of the studied dolerite outcrop (together with the swarm of igneous rocks in the Javalambre Sierra) seems responsible for a series of subtle magnetic anomalies that appear as normal dipoles aligned in a NW–SE direction.

Supplementary Material: Supplementary material is available at figshare.com (Oliva-Urcia, 2025).

Acknowledgements We acknowledge the financial support from projects PID2019-108753GB-C2 (C22 and C21) and PID2023-148256NB-I00 from MICIN/AEI/https://doi.org/10.13039/501100011033, "ERDF A way of making Europe" and the Aragon Government through the E32_20R (Grupo de Investigación Geotransfer). We are indebted to the Servicio General de Apoyo a la Investigación – SAI at the University of Zaragoza (particularly Laura de Juan and Raquel Moya for the preparation of thin sections) and personnel of the Earth Science Department for some of the analyses and sample preparation (Gregorio Sanz). We are indebted to F. Hrouda, his work (and team work) pushing the AMS instrumentation, AMS data in rocks and its interpretation in the geological realm but also for his kindness pointing out when "young" researchers are using the instrumentation "beyond" its design (particularly the use of the KLY3 with cooled standard samples to 77 K). We acknowledge reviewers R. Soto and P. Silva and Editor E. Petrovsky for their comments and suggestions, which substantially improved the first version of the manuscript.

Author Contributions Both authors contributed to the study conception and design. Field work, material preparation, data collection were performed by Antonio Casas-Sainz and Belén Oliva-Urcia, rock magnetic analysis were performed by Belén Oliva Urcia. The first draft of the manuscript was written by Antonio Casas-Sainz and Belén Oliva Urcia and all authors commented on previous versions of the manuscript. All authors read and approved the final manuscript.

Funding Open Access funding provided thanks to the CRUE-CSIC agreement with Springer Nature.

Data Availability Data is available upon request to the corresponding author.

Declarations

Open Access This article is licensed under a Creative Commons Attribution 4.0 International License, which permits use, sharing, adaptation, distribution and reproduction in any medium or format, as long as you give appropriate credit to the original author(s) and the source, provide a link to the Creative Commons licence, and indicate if changes were made. The images or other third party material in this article are included in the article's Creative Commons licence, unless indicated otherwise in a credit line to the material. If material is not included in the article's Creative Commons licence and your intended use is not permitted by statutory regulation or exceeds the permitted use, you will need to obtain permission directly from the copyright holder. To view a copy of this licence, visit http://creativecommons.org/licenses/by/4.0/.

References

Anadón P., Alcalá L., Alonso-Zarza A.M., Calvo J.P., Ortí F. and Rosell L., 2004. Cuenca de Teruel. In: Vera J.A. (Ed.), *Geología de España*. SGE-IGME, Madrid, Spain, 656–657 (in Spanish)

Aurell M., Fregenal-Martínez M., Bádenas B., Muñoz-García M.B., Élez J., Meléndez N. and De Santisteban C., 2019. Middle Jurassic-Early Cretaceous tectono-sedimentary evolution of the southwestern Iberian Basin (central Spain): Major palaeogeographical changes in the geotectonic framework of the Western Tethys. *Earth Sci. Rev.*, **199**, ArtNo.102983, https://doi.org/10.1016/j.earscirev.2019.102983

Caballero-Miranda C.I., Alva-Valdivia L.M., González-Rangel J.A., Gogitchaishvili A., Urrutia-Fucugauchi J. and Kontny A., 2016. Vertical AMS variation within basalt flow profiles from the Xitle volcano (Mexico) as indicator of heterogeneous strain in lava flows. *J. Volcanol. Geotherm. Res.*, **311**, 9–28https://doi.org/10.1016/j.jvolgeores.2016.01.003

Calvín P., Casas A.M., Villalaín J.J. and Tierz P., 2014. Reverse magnetic anomaly controlled by Permian Igneous rocks in the Iberian Chain (N Spain). *Geol. Acta*, **12**, 193–207, https://doi.org/10.1344/GeologicaActa2014.12.3.2

Cañón-Tapia E. and Pinkerton H., 2000. The anisotropy of magnetic susceptibility of lava flows: An experimental approach. *J. Volcanol. Geotherm. Res.*, **98**, 219–233, https://doi.org/10.1016/S0377-0273(99)00155-9

Cañón-Tapia E., 2004. Anisotropy of magnetic susceptibility of lava flows and dykes: A historical account. In: Martín-Hernández F., Lüneburg C.M., Aubourg C. and Jackson M. (Eds), *Magnetic Fabric: Methods and Applications*. Geol. Soc. London Spec. Publ. **238**, https://doi.org/10.1016/S0377-0273(96)00073-X

Cañón-Tapia E., 2004. Anisotropy of magnetic susceptibility of lava flows and dykes: A historical account. In: Martín-Hernández F., Lüneburg C.M., Aubourg C. and Jackson M. (Eds), *Magnetic Fabric: Methods and Applications*. Geol. Soc. London Spec. Publ. **238**, https://doi.org/10.1144/GSL.SP.2004.238.01.14

Chadima M. and Hrouda F., 2009. Cureval 8. Computer software. AGICO Inc., Brno, Czechia

Chadima M., Pruner P., Šlechta S., Grygar T. and Hirt A.M., 2006. Magnetic fabric variations in Mesozoic black shales, Northern Siberia, Russia: Possible paleomagnetic implications. *Tectonophysics*, **418**, 145–162, https://doi.org/10.1016/j.tecto.2005.12.018

Chadima M., Hrouda F. and Jelínek V., 2020. Anisoft 5. Computer software. AGICO Inc., Brno, Czechia

Cortés J.E., 2020. Volcanic rocks in Lower Jurassic marine carbonate successions in the southeastern Iberian Range (Spain): Biochronostratigraphic dating. *J. Iberian Geol.*, **46**, 253–277, https://doi.org/10.1007/s41513-020-00134-z

Cortés J.E., 2023. Dating volcanic materials through biochronostratigraphic methods applied to hosting strata (example from the Iberian Chain, eastern Spain). *C. R. Geosci.*, **355**, 175–201, https://doi.org/10.5802/crgeos.220

Das A. and Malik J., 2020. Applicability of AMS technique as a flow fabric indicator in dykes: Insight from Nandurbar-Dhule Deccan dyke swarm. *Int. J. Earth Sci.*, **109**, 933–944, https://doi.org/10.1007/s00531-020-01841-9

De Vicente G. and Vegas R., 2009. Large-scale distributed deformation controlled topography along the western Africa-Eurasia limit: Tectonic constraints. *Tectonophysics*, **474**, 124–143, https://doi.org/10.1016/j.tecto.2008.11.026

De Vicente G., Vegas R., Muñoz-Martín A., Van Wees J.D., Casas-Sainz A., Sopeña A., Sánchez-Moya Y., Arche A., López-Gómez J., Olaiz A. and Fernández-Lozano J., 2009. Oblique strain partitioning and transpression on an inverted rift: The Castilian Branch of the Iberian Chain. *Tectonophysics*, **470**, 224–242, https://doi.org/10.1016/j.tecto.2008.11.003

Dunlop D. and Özdemir Ö., 1997. *Rock Magnetism: Fundamentals and Frontiers*. Cambridge University Press, Cambridge, U.K.

Elming S.Å. and Mattsson H., 2001. Post Jotnian basic intrusions in the Fennoscandian Shield, and the break up of Baltica from Laurentia: A palaeomagnetic and AMS study. *Precambrian Res.*, **108**, 215–236, https://doi.org/10.1016/S0301-9268(01)00131-0

Ezquerro L., Lafuente P., Pesquero M.D., Alcalá L., Arlegui L., Liesa C., Luque L., Rodríguez-Pascua M.A. and Simón J.L., 2012. Una cubeta endorreica residual Plio-Pleistocena en la zona de

relevo entre las fallas de Concud y Teruel: Implicaciones paleogeográficas. *Rev. Soc. Geol. Esp.*, **25**, 157–173 (in Spanish)

Ferré E.C., Bordarier C. and Marsh J.S., 2002. Magma flow inferred from AMS fabrics in a layered mafic sill, Insizwa, South Africa. *Tectonophysics*, **354**, 1–23, https://doi.org/10.1016/S0040-1951(02)00273-1

García-Lasanta C., Oliva-Urcia B., Román-Berdiel T., Casas A.M., Gil-Peña I., Sánchez- Moya Y., Sopeña A., Hirt A.M. and Mattei M., 2015. Evidence for the Permo- Triassic transtensional rifting in the Iberian Range (NE Spain) according to magnetic fabrics results. *Tectonophysics*, **651**, 216–231, https://doi.org/10.1016/j.tecto.2015.03.023

García-Lasanta C., Román-Berdiel T., Oliva-Urcia B., Casas A.M., Gil-Peña I., Speranza F. and Mochales T., 2016. Tethyan versus Iberian extension during the Cretaceous period in the eastern Iberian Peninsula: Insights from magnetic fabrics. *J. Geol. Soc.*, **173**, 127–141, https://doi.org/10.1144/jgs2015-068

Gil-Imaz A., Pocoví A., Lago M., Galé C., Arranz E., Rillo C. and Guerrero E., 2006. Magma flow and thermal contraction fabric in tabular intrusions inferred from AMS analysis. A case study in a late-Variscan folded sill of the Albarracín Massif (southeastern Iberian Chain, Spain). *J. Struct. Geol.*, **28**, 641–653, https://doi.org/10.1016/j.jsg.2005.12.016

Gil-Imaz A., Lago-San José M., Galé C., Pueyo-Anchuela O., Ubide T., Tierz P. and Oliva-Urcia B., 2012. The Permian mafic dyke swarm of the Panticosa pluton (Pyrenean Axial Zone, Spain): Simultaneous emplacement with the late-Variscan extension. *J. Struct. Geol.*, **42**, 171–183, https://doi.org/10.1016/j.jsg.2012.05.008

Gómez J.J. and Fernández-López S.R., 2006. The Iberian Middle Jurassic carbonate- platform system: Synthesis of the palaeogeographic elements of its eastern margin (Spain). *Palaeogeogr. Palaeoclimatol. Palaeoecol.*, **236**, 190–205, https://doi.org/10.1016/j.palaeo.2005.11.008

Hoyer L. and Hasstie W.W., 2022. Variable magma flow in sills: Can a magma source be constrained? *J.* Volcanol. *Geotherm. Res.*, **421**, Art.No.107427, https://doi.org/10.1016/j.jvolgeores.2021.107427

Hoyer L. and Watkeys M.K., 2017. Using magma flow indicators to infer flow dynamics in sills. *J. Struct. Geol.*, **96**, 161–175, https://doi.org/10.1016/j.jsg.2017.02.005

Hrouda F., Buriánek D., Krejčí O. and Chadima M., 2015. Magnetic fabric and petrology of Miocene sub-volcanic sills and dykes emplaced into the SW Flysch Belt of the West Carpathians (S Moravia, Czech Republic) and their volcanological and tectonic implications. *J. Volcanol. Geotherm. Res.*, **290**, 23–38, https://doi.org/10.1016/j.jvolgeores.2014.12.001

Hrouda F., Ježek J. and Chadima M., 2020. Anisotropy of out-of-phase magnetic susceptibility as a potential tool for distinguishing geologically and physically controlled inverse magnetic fabrics in volcanic dykes. *Phys. Earth Planet. Inter.*, **307**, Art.No.106551, https://doi.org/10.1016/j.pepi.2020.106551

Hrouda F., Chadima M. and Ježek J., 2022. Anisotropy of out-of-phase magnetic susceptibility and its potential for rock fabric studies: A review. *Geosciences*, **12**, Art.No.234, https://doi.org/10.3390/geosciences12060234

Hrouda F., 2003. Indices for numerical characterization of the alteration processes of magnetic minerals taking place during investigation of temperature variation of magnetic susceptibility. *Stud. Geophys. Geod.*, **47**, 847–861, https://doi.org/10.1023/A:1026398920172

Jelínek V., 1981. Characterization of the magnetic fabric of rocks. *Tectonophysics*, **79**, T63–T67, https://doi.org/10.1016/0040-1951(81)90110-4

Kontny A., de Wall H., Sharp T.G. and Pósfai M., 2000. Mineralogy and magnetic behavior of pyrrhotite from a 260 C section at the KTB drilling site, Germany. *Am. Miner.*, **85**, 1416–1427, https://doi.org/10.2138/am-2000-1010

Lago San José M., Galé-Bomao C., Arranz-Yagüe E., Gil-Imaz A., Pocoví-Juan A. and Vaquer-Navarro R., 2000. The triassic alkaline dolerites of the Valacloche-Camarena area (SE-Iberian Chain, Teruel): Geodynamic implications. *Estudios Geol.*, **56**, 211–228

Liesa C.L., Casas A.M. and Simón J.L., 2018. La tectónica de inversión en una región intraplaca: La Cordillera Ibérica. *Rev. Soc. Geol. Esp.*, **31(2)**, 23–50 (in Spanish)

Lowrie W., 1990. Identification of ferromagnetic minerals in a rock by coercivity and unblocking temperature properties. *Geophys. Res. Lett.*, **17**, 159–162, https://doi.org/10.1029/GL017i002p00159

Lüneburg C.M., Lampert S.A., Lebit H.D., Hirt A.M., Casey M. and Lowrie W., 1999. Magnetic anisotropy, rock fabrics and finite strain in deformed sediments of SW Sardinia (Italy). *Tectonophysics*, **307**, 51–74, https://doi.org/10.1016/S0040-1951(99)00118-3

Majarena U., Lago M., Galé C. and Gil A., 2017. La intrusión de Cerro Redondo (Permico inferior, Cordillera Ibérica, Zaragoza): Reconstrucción 3D y modelo de emplazamiento. *Geogaceta*, **61**, 119–122 (in Spanish)

Martin S.A., Kavanagh J.L., Biggin A.J. and Utley J.E.P., 2019. The origin and evolution of magnetic fabrics in mafic sills. *Front. Earth Sci.*, **7**, Art.No.64, https://doi.org/10.3389/feart.2019.00064

Martín-Martín J.D., Gómez-Rivas E., Bover-Arnal T., Travé A., Salas R., Moreno-Bedmar J.A., Tomás S., Corbella M., Teixell A., Vergés J. and Stafford S.L., 2013. The Upper Aptian to Lower Albian syn-rift carbonate succession of the southern Maestrat Basin (Spain): Facies architecture and fault-controlled stratabound dolostones. *Cretac. Res.*, **41**, 217–236, https://doi.org/10.1016/j.cretres.2012.12.008

Nebot Miralles M. and Guimerà J., 2016. Structure of an inverted basin from subsurface and field data: the Late Jurassic-Early Cretaceous Maestrat Basin (Iberian Chain). *Geol. Acta*, **14**(2), 155–177, https://doi.org/10.1344/GeologicaActa2016.14.2.5

Oliva-Urcia B., 2025. Supplementary Material B Oliva and A Casas. figshare. Dataset. 10.6084/m9.figshare.30094933.v3

Ortí-Cabo F. and Vaquer-Navarro R., 1980. Volcanismo jurásico del sector valenciano de la Cordillera Ibérica. Distribución y trama estructural. *Acta Geológica Hispánica*, **XV(5)**, 127–130 (in Spanish)

Parés J.M. and van der Pluijm B.A., 2002. Phyllosilicate fabric characterization by low-temperature anisotropy of magnetic susceptibility (LT-AMS). *Geophys. Res. Lett.*, **29**, Art.No.2215, https://doi.org/10.1029/2002GL015459

Parés J.M. and van der Pluijm B.A., 2014. Low-temperature AMS and the quantification of subfabrics in deformed rocks. *Tectonophysics*, **629**, 55–62, https://doi.org/10.1016/j.tecto.2014.03.005

Petrovský E. and Kapička A., 2006. On determination of the Curie point from thermomagnetic curves. *J. Geophys. Res.-Solid Earth*, **111**, Art.No.B12S27, https://doi.org/10.1029/2006JB004507

Pueyo Anchuela Ó., Ramajo Cordero J., Gil Imaz A., and Meléndez Hevia G., 2013. Analysis of anisotropy of magnetic susceptibility in iron-oolitic beds: a potential tool for paleocurrent identification. *Int. J. Earth Sci.*, **102**, 1131–1149, https://doi.org/10.1007/s00531-012-0848-2

Raposo M.I.B., 1997. Magnetic fabric and its significance in the Florianópolis dyke swarm, southern Brazil. *Geophys. J. Int.*, **131**, 159–170, https://doi.org/10.1111/j.1365-246X.1997.tb00602.x

Simón-Muzás A., Casas-Sainz A.M., Soto R., Gisbert J., Román-Berdiel T., Oliva-Urcia B., Pueyo E.L. and Beamud E., 2022. Axial longitudinal flow in volcanic materials of the Late Carboniferous-Permian Cadí basin (Southern Pyrenees) determined from anisotropy of magnetic susceptibility. *J. Volcanol. Geotherm. Res.*, **421**, Art.No.107443, https://doi.org/10.1016/j.jvolgeores.2021.107443

Simón-Muzás A., Casas-Sainz A., Soto R., Beamud E. and Gisbert J., 2023. Dyke or pipe? Contributions of magnetic fabrics to the reconstruction of the geometry of an eroded subvolcanic body (Cadí basin, Pyrenees). *J. Struct. Geol.*, **172**, Art.No.104891, https://doi.org/10.1016/j.jsg.2023.104891

Soriano C., Beamud E., Garcés M. and Ort M.H., 2016. 'Anomalous' magnetic fabrics of dikes in the stable single domain/superparamagnetic threshold. *Geophys. J. Int.*, **204**, 1040–1059, https://doi.org/10.1093/gji/ggv495

Valenzuela-Ríos J.I., Martínez-Rodríquez R.M. and Lago-San José M., 1996. Nota preliminar sobre la edad del paleovolcanismo jurásico de Javalambre (Cordillera Ibérica, Teruel). *Geogaceta*, **19**, 39–40 (in Spanish)

Zhang Q. and Appel E., 2023. Reversible thermal hysteresis in heating-cooling cycles of magnetic susceptibility: A fine particle effect of magnetite. *Geophys. Res. Lett.*, **50**, Art.No.e2023GL102932, https://doi.org/10.1029/2023GL102932

Ziegler P.A., 1990. Collision related intra-plate compression deformations in Western and Central Europe. *J. Geodyn.*, **11**, 357–388, https://doi.org/10.1016/0264-3707(90)90017-O